



POROTECH Ltd.
Ontario, Canada

**THE METHOD OF STANDARD
POROSIMETRY
AND
AUTOMATED STANDARD POROSIMETER**

Professor Y. M. Volfkovich et al.

**POROTECH Ltd.,
4 Director Court, Woodbridge Court,
Ontario, Canada
L4L 3Z5 Tel: [905-482-2037](tel:905-482-2037)
Fax: 866-686-4404 email: porotech@magma.ca**

ABSTRACT

A new method of Standard Porosimetry (MSP) for investigation of any type of porous materials, including soft, frail materials, and powders is developed. The method is relatively simple and nondestructive, and can be used for measurements in a wide range of pore sizes from 1 to $3 \cdot 10^6$ nm. This method can also be used for evaluation of wetting angles and water wettability of multi-component porous materials.

Experimental data from the MSP application in studies of different processes in batteries, fuel cells, and other electrochemical devices are discussed. The following processes were investigated: swelling of ion-exchange polymeric materials (membranes, conducting polymers); pressing of powdered materials (PVC, Raney silver); influence of the temperature on the porous structure; influence of the pore-forming agents; chemical and electrochemical sintering of catalysts; deposition of solid products in the pore space of the cathode during reduction of SOCl_2 in lithium batteries; structural changes during the formation and cycling of lead and silver oxide electrode, etc.

The MSP employs numerous manual operations. In order to avoid the ones, the Automated Standard Porosimeter (ASP) was developed based on the MSP. This ASP consists of: electronic balance, automatic manipulator, device for drying of the porous samples with a flow of dry inert gas controlled by an electromagnetic valve, and computer. The serial production of Automated Standard Porosimeter is planned by POROTECH, Inc. in the nearest future.

INTRODUCTION

The structural and surface properties of porous materials used in different electrochemical devices (electrodes, separators, membranes, catalysts, active components in batteries, fuel cells, electrolyzers, sensors, etc.) have a great influence on the performances of these devices. The knowledge of structural properties is important also for many other

materials, such as ceramics, powder-metallurgical products, soils, oil- or gas-bearing strata and rocks, construction materials, etc.

The porous structure can be characterized by integral or differential curves of pore volume distribution vs. pore radius (porosimetric curves or porograms). The following methods for measuring porograms are well known: mercury porosimetry - mercury intrusion into a nonwetttable porous material [1]; small-angle X-ray scattering [2]; electronic or optical microscopy; centrifugal porosimetry [3]; displacement of wetting liquids from the pore volume by gas pressure [4]; capillary condensation [5].

Each of these methods has its own advantages and limitations. Small-angle X-ray scattering can be used only for pore radii ranging from 2 to 50 nm and often leads to ambiguous results. Centrifugal porosimetry, optical microscopy, and displacement methods are practically useless for $r < 10^3$ nm. Measurements by electronic microscopy are associated with difficulties in pretreatment of the samples and in interpretation of the results. The method of capillary condensation can be used in the pore size range from 1 to 50 nm only.

The method of mercury porosimetry (MMP) provides the widest range of measurable pore radii (from 2 to 10^5 nm). Great disadvantage of this method is the necessity to apply high pressure of mercury (up to thousands of atmospheres), which can lead to deformation or even destruction of the samples and to distortion of the porograms [5-7]. Other drawbacks of this method are: misrepresentation of the results due to amalgamation of most metals [8], different values of the mercury wetting angle for different materials [7], complexity of the equipment, toxicity of mercury.

In the A. N. Frumkin Institute of Electrochemistry of the Russian Academy of Sciences, a new method of standard porosimetry (MSP) was developed. Most of the above mentioned disadvantages are eliminated with the use of the MSP. In addition, it enables measurements in a large range of pore sizes and with different kinds of materials including soft or frail materials, as well as materials forming amalgams [9-18].

PRINCIPLES OF THE METHOD

The method is based on the laws of the capillary equilibrium. If two (or more) porous bodies partially filled with a wetting liquid are in state of capillary equilibrium, then the values of the capillary potentials ψ_i for these bodies are equal:

$$\psi_1 = \psi_2 = \dots \psi_i \equiv \psi \quad (1),$$

where ψ_i is the capillary potential for the i^{th} body.

The MSP measures the dependence of the equilibrium on the relative liquid content, i.e. the volume of liquid (V_t) in the test sample as a function of the volume of liquid (V_s) in the standard samples:

$$V_t = \phi (V_s) \quad (2).$$

Prior to the measurement, the integral liquid distribution in terms of ψ for the standard sample is established,

$$V_s = f_s (\psi) \quad (3).$$

From equations (1) to (3), the liquid distribution in terms of ψ for the test sample is obtained:

$$V_t = \phi [f_s (\psi)] \quad (4),$$

the equilibrium state being attained by liquid and vapor flow. These transport effects are caused by gradients of the capillary potentials formed by: the capillary pressure p_c and the relative vapor pressure of the liquid $\tilde{p} = p_s / p_o$ (where p_s designates the vapor pressure of the liquid in the system and p_o the saturated vapor pressure). The capillary pressure can be represented by the Laplace equation:

$$p_c = -2\sigma \cos \theta / r_m \quad (5),$$

where σ is the surface tension of the liquid, θ is the wetting angle, and r_m is the maximum radius of pores filled with liquid. Using the value of p_c as a capillary potential, one can derive from equations (4) and (5) the radial pore distribution function:

$$V_t = \phi [f_s (-2\sigma \cos \theta / r)] \equiv F (r) \quad (6).$$

Employing a measuring liquid with $\theta \sim 0$ (wetting liquid) from (6) one obtain:

$$V_t = \phi [f_s (-2\sigma / r)] \equiv F (r) \quad (7).$$

An example of liquid distribution in two porous bodies for such a case is given in Fig. 1.

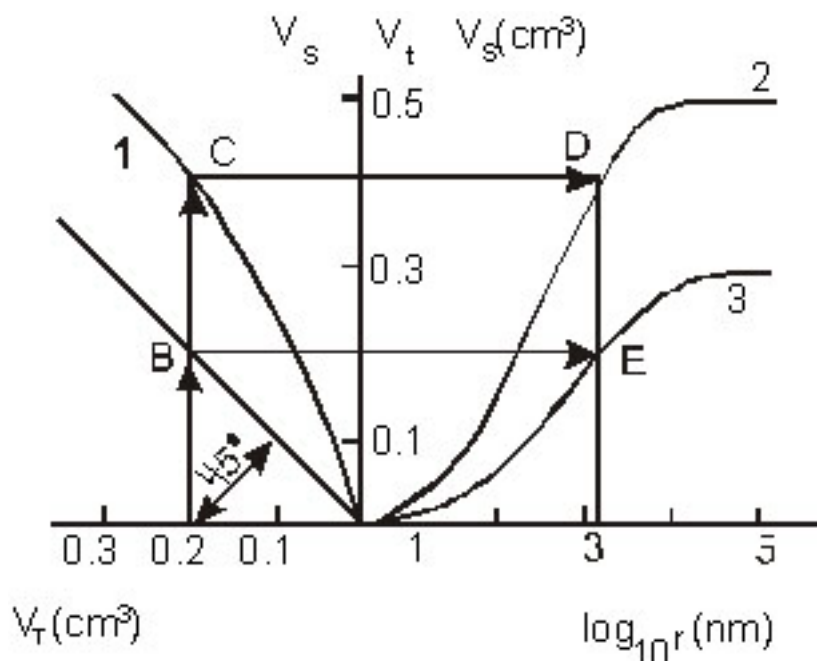


Fig. 1:

Examples for determination of pore size distribution curves by MSP: (1) V_s vs. V_t ; pore size distribution curves for the standard sample (2) and for the test sample (3).

On the left, curve 1 represents the experimental dependence of the volume V_s in the standard sample on the volume V_t in the test sample for different values of V_o ($V_o = V_s + V_t$). On the right, the integral pore size distribution curves (pore volume as a function of $\log r$) are shown. Curve 2 is the known curve for the standard sample. Let us assume, for simplicity, that the wetting angles of the liquid for both bodies are equal. For a certain total volume of liquid V_o' , the volumes of liquid in both bodies V_s' and V_t' are represented by the coordinates of point C. This point corresponds to point D on curve 2 and to a certain value r' of the maximum radius of filled pores. In the case of capillary equilibrium (under the assumption made), the maximum radius of filled pores in the test sample will be the same. As in this sample the volume of liquid is represented by point B (the line is drawn at an angle of 45°), the point E corresponds to a point on the pore size distribution curve for the test sample. Thus, changing the value of the total volume V_o of the liquid, the overall distribution curve 3 for the test sample can be determined. The specific surface area (S), which is an important

parameter of the porous structure, can be obtained from the integral pore radius distribution curve using expression (8):

$$S = 2 \int_0^{\infty} (1/r)(dV/dr)dr \quad (8).$$

EXPERIMENTAL

Method of measurement

The amount of liquid in the samples is determined by weighing. As a working liquid, hydrocarbons (octane, decane, etc.) usually are used, which completely wet most of the materials ($\theta \sim 0^\circ$). Thus the assumption of equal wetting angle is fulfilled. In some cases other liquids are used, e.g. water.

The porous standards and the test sample are prepared in the shape of discs with thickness of 0.1-3 mm. They are washed, dried, and weighed. Then they are filled with the liquid (under vacuum). The stack of discs is assembled in a special clamping device (Fig. 2), in which they are tightly attached to each other for attainment of capillary equilibrium. In the case of easily compressible (soft) materials the pressure must be controlled (e.g., by sylphon bellows). In the assembly, the test sample (1) is usually placed between two standard samples (2). A small portion of the liquid is evaporated off this assembly through the open surface (3) by heating and/or vacuum treatment or by a flow of a dry inert gas. When certain amount of liquid is removed, the open surface of the samples is hermetically covered and left undisturbed for a certain time (1-30 minutes) to allow the establishment of a new capillary equilibrium. Subsequently, the stack is disassembled, the samples are placed into individual vials and weighed. Then the stack is reassembled and all operations repeated several times until the liquid from the test sample is completely evaporated.

Other possibilities for changing the total volume of the liquid exist, e.g., by repeatedly contacting the test sample with standard samples containing different amounts of liquid.

The attainment of capillary equilibrium can be controlled by the use of two standard samples, one of which is placed at the open surface of the stack (where the liquid evaporates) and the other one at the closed surface. If during the experiment the amount of liquid in both

standard samples corresponds to their known distribution curves then equilibrium is established throughout the whole stack. In the case of samples with small pores (<10 nm), the disassembling of the stack is performed in a dry box in order to prevent adsorption of humidity from the air. When samples with large pores ($>10^4$ nm) are analyzed, the stack is disassembled in a box saturated with vapor of the measuring liquid in order to avoid drying of the stack.

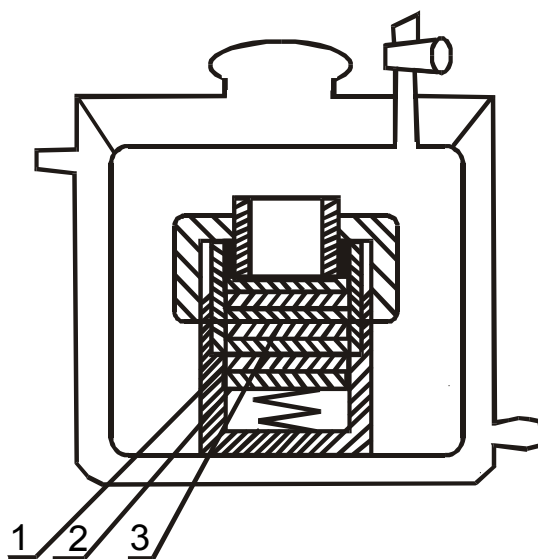


Fig. 2: Clamping device: (1) test samples; (2) standard samples; (3) open stack surface.

Using this method, porograms can be measured for powdered materials as well. These materials are placed between two sheets of filter paper. Other samples of filter paper with no powder are also assembled in a stack. The pore volume distribution curve for the powder can be determined by subtracting the porograms of the "empty" filter paper samples from the ones of the test sample. Capillary equilibrium between different porous samples can also be established through vapor phase (with no direct contact of the samples), the so-called method of contactless standard porosimetry. However, in this case the time for establishing of the equilibrium increases considerably. The pore size distribution of the standard samples is to be determined by other methods, e.g., by mercury porosimetry. The materials used must be

sufficiently hard and must not be deformed and amalgamated by mercury, e.g., nickel or ceramic materials. The standard samples must possess sufficiently high pore volume in the pore size range of interest as to allow accurate measurement of the mass increase during flooding of these pores. The time needed for the measurement of a porogram depends on the pore properties of the sample (which determine the time of the equilibrium establishment) and varies between 2 and 10 hours.

RESULTS AND DISCUSSION

1. Limitations, accuracy and sensitivity of the method

MSP with appropriate standard samples can be used for measurements of pore sizes in the range from 1 to $3 \cdot 10^6$ nm. The accuracy of MSP depends primarily on the accuracy of measuring the pore size distribution curve of the standard samples. The accuracy of the method of Mercury Porosimetry (MMP) in measuring of such curve is about 1% of the total pore volume. As was shown by special experiments, under suitable conditions the error (nonreproducibility) of the MSP is less than 1%.

The sensitivity of the method is illustrated in Fig. 3, which represents the results for several practically monolithic samples of carbonate rocks (porosity less than 1%). Related to the total volume of the sample, the sensitivity in this case was 0,05-0,07%.

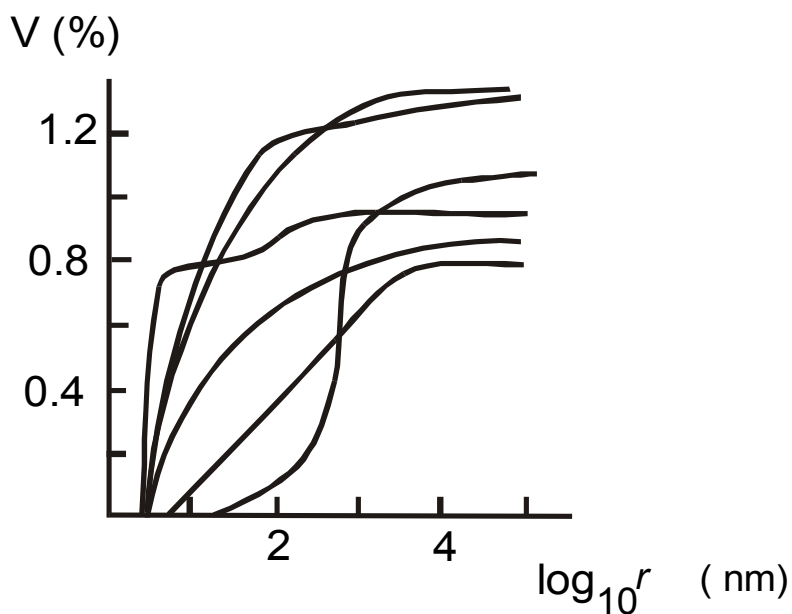


Fig. 3: Integral porograms for different carbonate rocks from the Vuktyl region [19].

In Fig. 4, porograms obtained by MSP and MMP of different types of electrodes are shown. It can be seen that the results by these two methods are in a good agreement. Here $v = V/V_0$ is the relative pore volume, where V is the pore volume, and V_0 the total volume of the test sample.

2. Porosimetry of samples prone to deformation

Sometimes MMP is used for investigation of low-mechanical-strength samples [6, 7]. To evaluate the influence of the high mercury pressure, results of measurements by MMP and MSP for such samples were compared. The deformation effect depends on the nature of the material. As an example, in Fig. 5 differential porograms are shown for a fibrous filter material FPIAN-5, which is used as a separator in batteries. It can be seen that the sample deformation alters the shape of the curves: the number and the position of the maxima on these curves are different. They coincide only in the pore size range of $10^2 - 10^3$ nm, which points on a rigid microporous structure within the fibers.

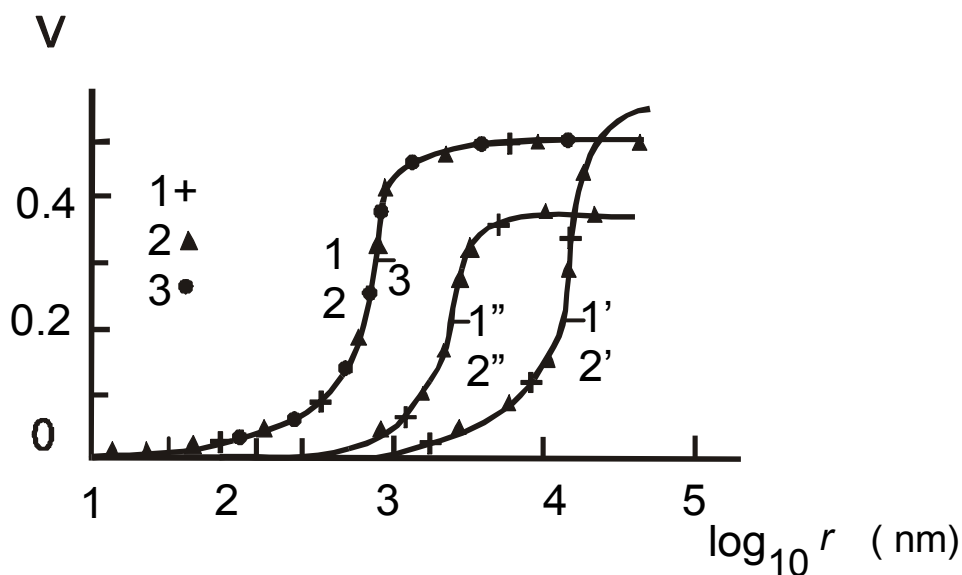


Fig. 4: Integral porograms obtained by MSP (1, 1', 1''), MMP (2, 2', 2''), and contactless MSP (3) for porous electrodes prepared from a mixture of carbonyl and Raney nickel (1 - 3), carbonyl nickel (1'', 2''), and titanium (1'', 2'') [18].

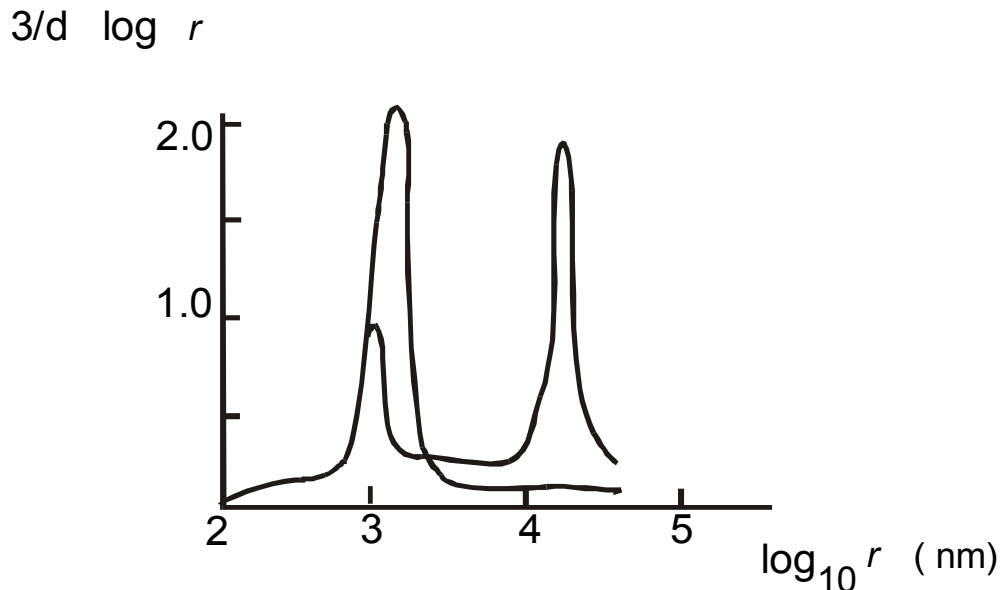


Fig. 5: Differential porograms obtained by MSP (1) and MMP (2) for FPIAN-5 filters [18].

MSP enables measurements of samples at fixed levels of compression, i.e., under conditions they are commonly used in different devices. Porograms at different levels of compression reveal additional information on the properties of the porous structure.

It should be noted as well that MSP allows repetitive measurements on the same sample at different external conditions, e.g., of an electrode at different depths of charge or discharge, which gives the possibility to investigate structural changes. Indeed even for soft or frail materials there is no deteriorative influence of the measurement on the sample (in contrast to MMP) and after drying up the latter fully retains its previous structure.

3. Measurement of the total pore volume

When the total porosity of porous bodies is measured, an error often occurs due either to a thin liquid film on the sample surface or to a deficiency of liquid following attempts to remove this film. On the base of MSP a method for measurement of the total pore volume was developed [18] employing a new procedure of filling the sample with wetting liquid. The test sample is contacted with an auxiliary sample whose volume of coarse pores V_2 is higher

than the total volume of the test sample V_1 . Then liquid is added to the samples at volume higher than V_1 , but lower than V_2 . At these conditions the pores of the test sample will be completely filled with the liquid while no film is formed on the sample surface.

4. Analysis of samples with corrugated pores

Corrugated pores affect to a great extent processes of mass- and heat-transfer and the current flow in porous materials. For samples with corrugated pores, the porograms measured in opposite directions usually do not coincide, therefore it is difficult to evaluate the true shape of the porogram. MSP gives the possibility to measure the true pore size function, which is not influenced by the pore corrugation [15, 18]. The quantitative expression of such a porous structure is given by the statistical distribution of the volume of the trapped (blocked) pores V_{tr} vs. both their radii r_{tr} and the radii of the blocking pores (necks) r_b :

$$F(r_{tr}, r_b) \equiv \partial^2 V_{tr} / \partial r_{tr} \partial r_b \quad (9).$$

To evaluate this function it is necessary to measure the porograms by two modes: a) by filling of the pores with liquid, and b) by evaporation of the liquid starting from different degrees of filling. In Fig. 6, a set of porograms for an electrode from carbonyl nickel is shown. In Fig. 7, in coordinates $\log r_b$, $\log r_{tr}$ the lines connect points with equal values of the distribution function (dimensionless, for relative porosity). The line with 45° angle is characteristic for sample with no corrugation. From this figure it follows that the pores of this electrode could be subdivided into 3 groups: 1) coarse pores with radii 30-70 μm and low degree of corrugation, formed by special pore-forming additives, 2) pores in the range 2-15 μm with high degree of corrugation, located between particles of the carbonyl nickel, and 3) a low volume of small pores (below 1 μm) with low degree of corrugation, located inside the nickel particles. Such type of distribution function has not been described in the literature yet.

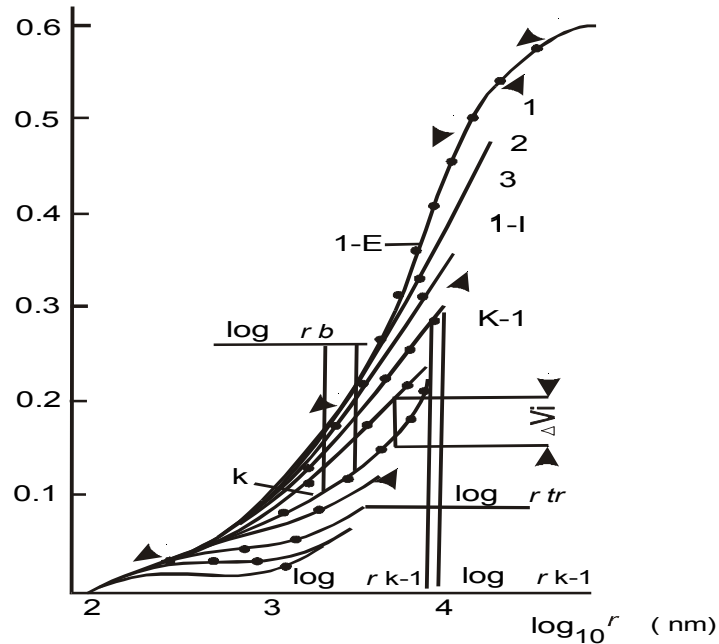


Fig. 6: Integral porograms for electrodes made from carbonyl nickel measured by MSP via: (1-I) capillary impregnation, (1-E) evaporation starting from complete flooding, and (1, 2, ...k-1, k) evaporation starting with different degrees of flooding [18].

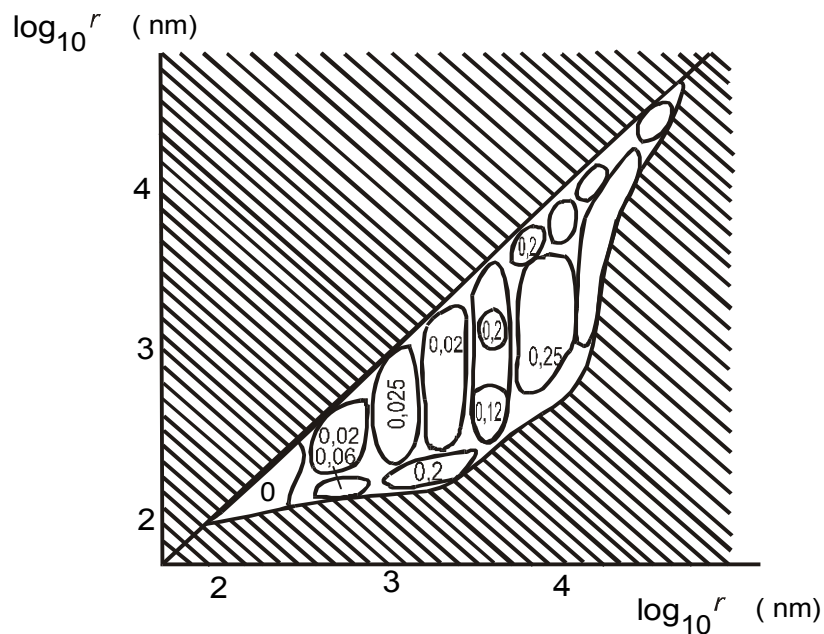


Fig. 7: The volume-distribution function of blocked pores in terms of the logarithms of their radii (r_{tr}) and of the logarithms of the radii of blocking pores (r_{bl}) calculated from the programs shown in Fig.6 [18].

5. Measurement of wetting angles

The measurement of wetting angles for porous materials is associated with some difficulties particularly if these materials cannot be prepared with a smooth surface (e.g., carbons, soil samples, construction materials, etc.). MSP allows measurements of wetting angles within the broad range of θ from 0° to 90° . For this purpose porograms are measured with both the test liquid whose wetting angle should be determined and the standard liquid whose wetting angle is known (e.g., hydrocarbons with $\theta \sim 0^\circ$). The results are plotted as indicated above, i.e. without taking into account the change of the value of $\cos \theta$. In this case the curves for the two liquids will be shifted along the $(\log r)$ -axis. For a given amount of liquid V' the capillary pressure (the value of $\cos \theta/r$) in both cases will be the same. Therefore the value of the shift will be $\log [\cos \theta_t / \cos \theta_s]$ or, when $\theta_s \sim 0^\circ$, $\log \cos \theta_t$. If the value of θ_t for the sample is not constant but depends on the pore size, then some deformation of the porogram will be present along with the shift. From the values of the shift for different values of V_t the dependence of θ_t on the pore size can be found. In Fig. 8 porograms are shown for a porous sample of pressed PTFE powder in cyclohexanone, isopropyl alcohol, and decane. One can see that there is an almost parallel shift of the curves without deformation. Assuming that for decane $\theta_s \sim 0^\circ$ we find for cyclohexanone $\theta_t = 52^\circ$ and for isopropyl alcohol $\theta_t = 20^\circ$. These values are close to the values measured on a smooth PTFE surface [20].

The situation is different for samples of activated carbon. In Fig. 9, porograms for carbon samples SKN-1 and SKN-4M in decane and water are presented. It is evident that the micropores are practically hydrophilic. Increase in the pore radius up to 10 nm is accompanied by reduced wettability with water (the wetting angle θ_t increases). Almost all the pores with $r > 10$ nm are hydrophobic.

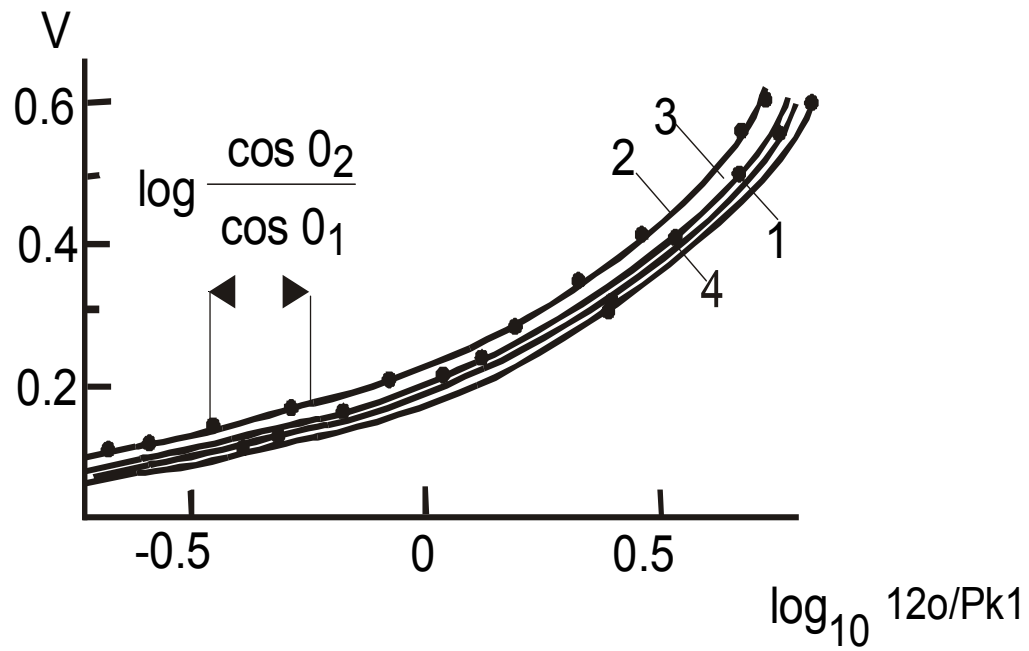


Fig. 8: Integral porograms of a porous PTFE sample measured by MSP with: (1) cyclohexanone, (2) isopropyl alcohol, and (3) decane, and (4) measured by MMP [10].

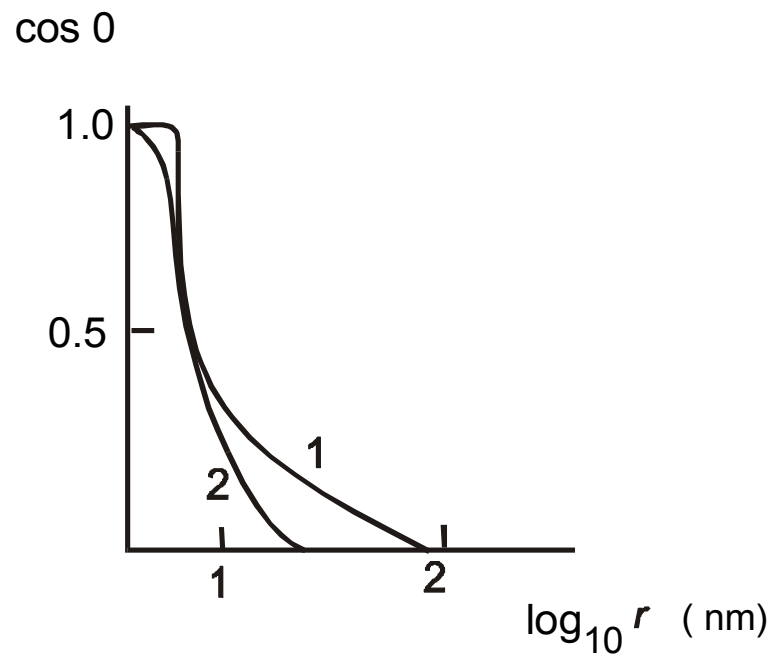


Fig. 9: Wetting angle of water vs. pore size for active carbon adsorbents SKN-1K (1) and SKN-4M (2) [21].

6. Analysis of multi-component porous samples

Multi-component porous materials with mixed wettability in water (hydrophobic-hydrophilic materials) are widely used as electrodes in fuel cells and other electrochemical devices, as well as in other fields (glass-reinforced plastics, composite materials, etc.). MSP provides complete information on the structure and surface properties of such materials. For this purpose measurements are performed with several liquids with a different wettability of each component of the material. Let us consider a two-component catalytic active electrode system consisting of platinum black and PTFE particles. Let us denote the wetting angle of water with the hydrophilic and the hydrophobic component as θ_1 and θ_2 , respectively. Such a material contains hydrophilic pores between the Pt particles, hydrophobic pores between the PTFE particles, and pores with mixed properties, which are filled with water only if for an average value of $\cos \theta$ the condition

$$\cos \theta \equiv ((1 - \rho) \cos \theta_1 + \cos \theta_2) > 0 \quad (10)$$

is fulfilled [22]; here ρ is the fraction of the pore surface occupied by the hydrophobic component (PTFE).

To evaluate the structure of this electrode it was wetted in different liquids with $\theta = 0^\circ$ with platinum and the dependence of the amount of liquids in the electrode was measured as a function of their wetting angles with PTFE θ_p by hydrostatic weighing.

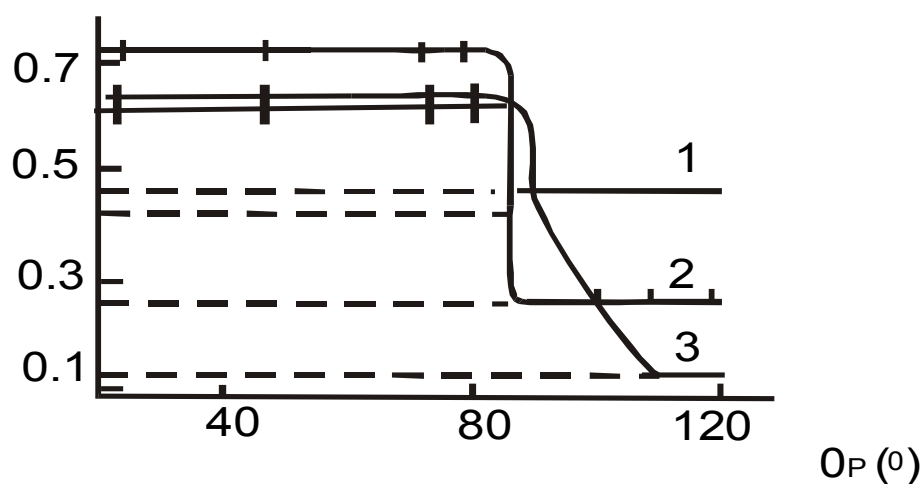


Fig. 10: Flooding degree vs. wetting angle with different liquids for electrodes of: (1) platinum + 6% PTFE; (2) platinum + 16% PTFE, and (3) nickel + 4.8% PTFE [17].

Fig. 10 shows that this dependence is step-like. In the range of θ_p from 24 to 90° the amount of liquid remains unchanged at a value equal to the total porosity of the electrode (curves 1 and 2). This result testifies on small amount of mixed pores in this particular case, while in the case of the electrode containing carbonyl nickel and PFTE a sloping section appears on the curve indicating existence of mixed pores (curve 3).

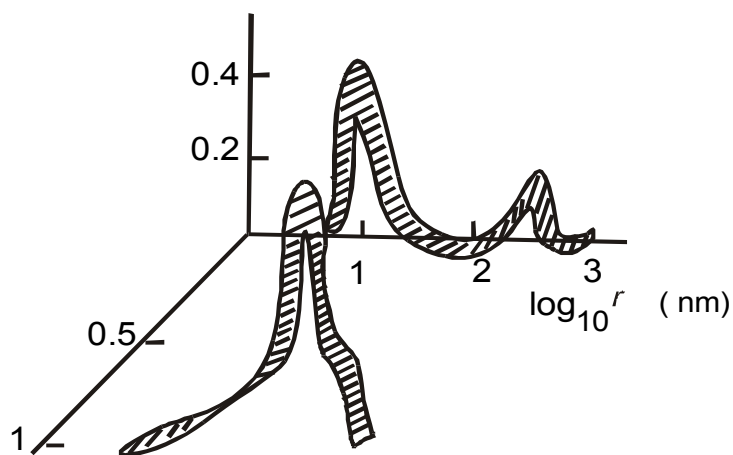


Fig. 11: Differential pore-distribution function in terms of radii and hydrophobicity factors p for a platinum electrode containing 16% PTFE [17].

From the porograms obtained with different liquids, differential distribution functions of the pore volume vs. pore radius and ρ -values, $\partial^2 V / \partial \rho \partial \log r$, were calculated (Fig. 11, for a layer containing 16% PTFE). It can be seen that this function has three maxima - two for hydrophilic and one for hydrophobic pores. Such kind of functions has not been described yet in the literature.

MSP was applied as well for investigation of two-component negative electrodes of solid-oxide fuel cells (SOFC), consisting of nickel particles and solid electrolyte particles [23].

7. Adsorption isotherms

The ability of highly dispersed (colloidal) porous systems to adsorb or to release liquids can be probed by the method of capillary condensation. It is usually characterized by adsorption isotherms, i.e. equilibrium relations between the amount of liquid bound to the body and the relative vapor pressure of the liquid $\tilde{p} = p_s/p_o$, where p_s designates the vapor pressure of the liquid in the system and p_o is the saturated vapor pressure. The upper limit for this method is at pore size of about 50 nm, where $p_s \sim p_o$.

By using standard porosimetry measurements it is possible to extend the term of adsorption isotherms to a broader range of porous systems. For this purpose it is convenient to use the parameter "free binding energy liquid-sample" (capillary potential, differential work of wetting). This parameter, designated here by A , is related to the structural (r) and surface properties (θ) of the system, which can be determined by MSP and also through the relative vapor pressure (the method of capillary condensation) via the Kelvin equation:

$$A = -RT \ln (p_s/p_o) = 2\sigma \cos \theta V_m/r \quad (11).$$

Adsorption or desorption isotherms expressed as function of the amount of liquid in the system on the free binding energy allow to compare the behavior of any kind of porous systems, studied by different methods, even of lyophobic systems for which A has negative values. A few water desorption isotherms are presented in Fig. 12 as plots of the volume of filled pores vs. A , as well as, for comparison, vs. \tilde{p} and vs. r .

Very diverse samples have been examined including hydrophilic, hydrophobic and mixed materials, typically porous samples and samples of colloidal type (pine wood, peat). The spectrum of A values measured is rather wide here: six orders of magnitude in the hydrophilic region and three orders of magnitude in the hydrophobic region. It can be seen that isotherms measured by MSP give complete information concerning the uptake of liquids by porous systems.

8. Automation of measurements. Automated Standard Porosimeter

The MSP described above implies numerous manual operations: multiple assembling and disassembling of the stack, weighing of the individual test and standard samples, etc. In order to minimize manual operations, an Automated Standard Porosimeter (ASP) based on the MSP was developed. This ASP consists of the following components: electronic balance

«Sartorius» for weighing of the test and standard samples; an automatic manipulator for the assembling and disassembling of the stack of samples and for transfer of the samples to the balance; device for drying of the samples stack by a flow of dry inert gas controlled by an electromagnetic valve and computer for management of measuring process, data acquisition and processing. Serial production of such Automated Standard Porosimeter is planned by POROTECH, Inc. in the nearest future.

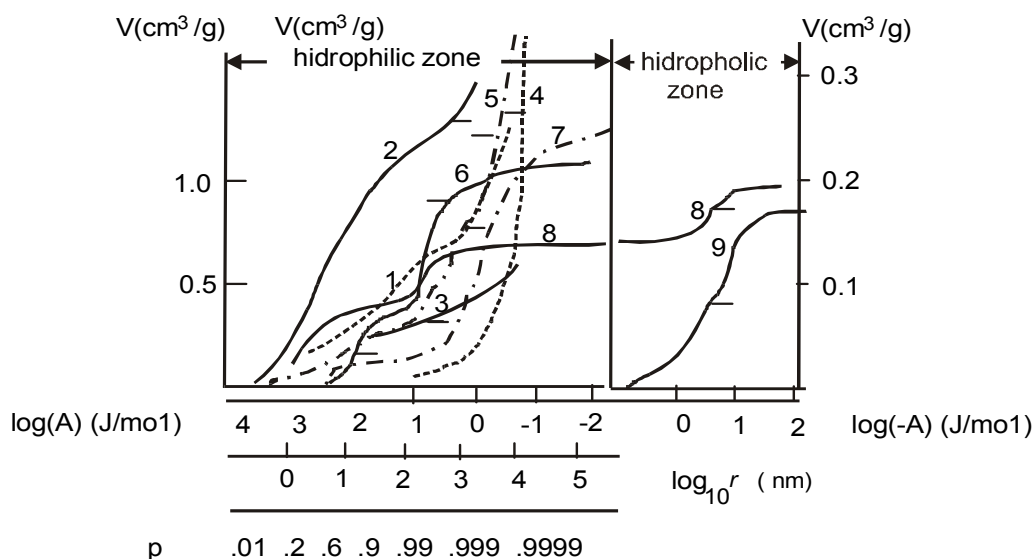


Fig. 12: Integral water volume-distribution curves in terms of $\log A$, $\log r$, and p for: (1) milled peat; (2) red clay; (3) pine wood; (4) quartz sand; (5) filter paper; (6) an activated carbon electrode; (7) a porous nickel electrode, (8) a porous platinum electrode with PTFE, and (9) a PTFE filter [18].

9. Study of formation of porous structures

The processes of formation of porous structures with desired properties and of modification of the porous structure affected by external factors or by technological processing are not as yet studied in detail. One of the reasons for this is the fact that the most applicable porosimetric method, the method of mercury porosimetry (MMP), is destructive and does not allow repetitive measurements of the same sample. The MSP and ASP provide serious advantage from this point of view.

9. 1. Nondestructive measurements of structural changes

The opportunity of repetitive measurements of the same sample excludes, for instance, the influence of technological nonreproducibility of the parameters of different samples and substantially increases the accuracy and sensitivity of the measurements. This can be illustrated by the results of measurements on the negative electrode of lead-acid batteries [24]. At different stages of their functioning the cells were disassembled, one of the negative electrodes was washed, dried and placed in a special device for porosimetric measurements. After the measurements, the electrode was reassembled in the cell for further cycling. In Fig. 13, porograms of three electrodes after initial discharge at -20°C are shown.

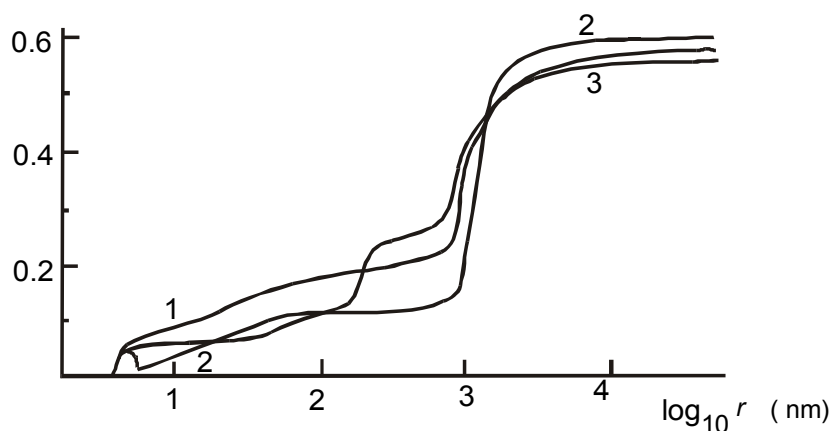


Fig. 13: Integral porograms of three lead electrodes after initial discharge at -20°C [2].

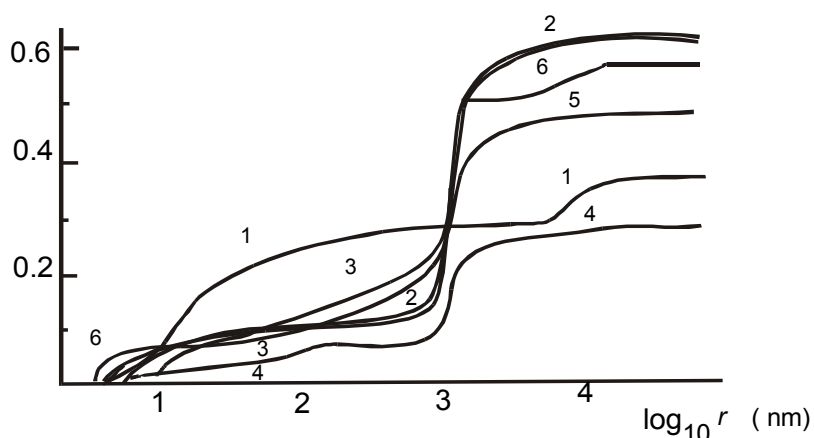


Fig. 14: Integral porograms of lead electrodes at different stages of manufacturing and cycling: (1) pasting; (2) formation; (3) charge; (4) discharge at low current density; (5) initial discharge at $+20^{\circ}\text{C}$, and (6) -20°C (2).

One can see that the technological scattering of the structure is comparable with the changes of the structure under the influence of some of these processes.

9.2. Swelling of porous materials

When an insufficiently rigid porous material is soaked with a wetting liquid, there is possibility of a volume increase (swelling) due to the capillary pressure p of the liquid. If such a material is used in a liquid medium, it is important to know how its porous structure is affected in this medium. The swelling process depends on the nature of the liquid. In the absence of a specific interaction between the porous material and the liquid, the capillary pressure is proportional to the surface tension of the liquid.

The structure of chrysotyl asbestos, which is widely used as separator in various electrochemical devices (electrolyzers, fuel cells, etc.) was studied. As working liquids octane ($\sigma = 21,7 \text{ mJ/m}^2$), water ($\sigma = 72,5 \text{ mJ/m}^2$) and a 7M solution of KOH ($\sigma = 92 \text{ mJ/m}^2$ [25]) were used. For alkaline solutions the method described above is inapplicable because due to water evaporation or condensation the solution concentration is changed. A modified method was developed in which the amount of liquid in the porous samples is changed by capillary soaking or drying. In the former case, the dried test sample is contacted with several standard samples filled with different amounts of liquid. In the latter case, a completely filled test sample is contacted with dried standard samples. In Fig. 15, differential porograms obtained by this method are shown. In octane (curve 1) there is practically no swelling of the asbestos and the porogram is characteristic for its native porous structure. In water (curve 2) swelling is detected as a result of increase of the volume of pores with radii in the range from 10^3 to $4.5 \cdot 10^4 \text{ nm}$. In alkaline solution (curve 3) there is further volume increase in the range of the largest pores.

In the case of ion exchange membranes (solid polymer electrolytes) different type of swelling can be observed. For the anion exchange membrane MA-100 in water the pore volume increases almost by an order of magnitude mainly as a result of formation of pores smaller ($<10 \text{ nm}$) than those in the dry membrane (Fig. 16).

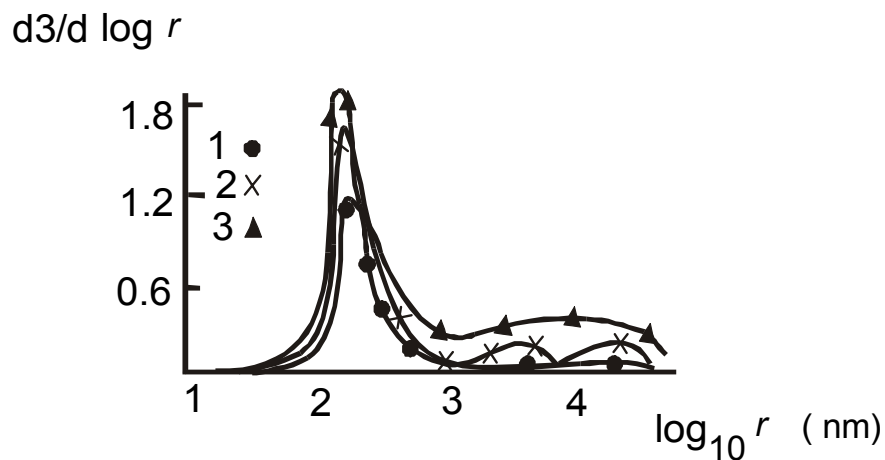


Fig. 15: Differential porograms of asbestos with different liquids: (1) octane, (2) water, and (3) 7M KOH.

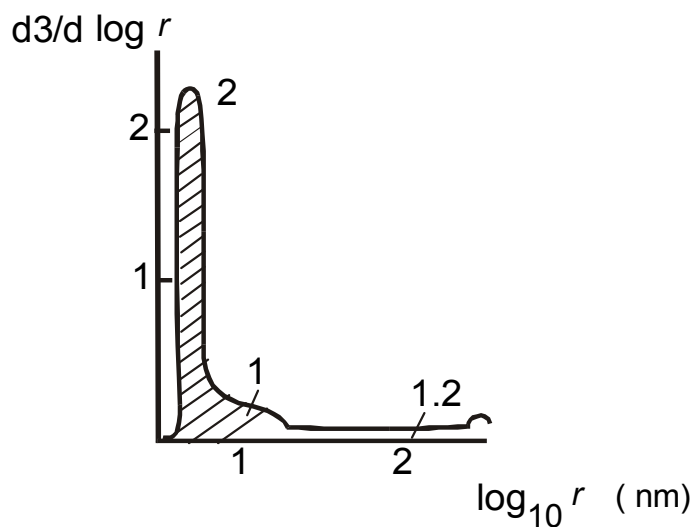


Fig.16: Differential porograms of ion-exchange membrane MA-100 measured by evaporation of (1) octane and (2) water.

The same behavior exhibit in water some conductive polymers like polyaniline and poly(para-phenylene).

MSP was also applied for investigation of swelling processes of different conductive polymers in acetonitrile and γ -butyrolactone (GBL) [26, 27].

9.3. Influence of preliminary soaking and evaporation. Memory effects

When the porous structure of polyaniline in the form of emeraldine chloride or sulfate is studied, a peculiar "memory" effect can be observed which appears as a well-pronounced shape change of the porograms during consecutive measurements with water as a working liquid (Fig. 17) [28]. As a result of pore volume increase in the micropore range, the specific surface of the sample increases substantially. A similar behavior was observed for the system poly(para-phenylene)-acetonitrile [29]. This phenomenon can be tentatively explained by a loosening and subsequent shrinkage of the labile porous structure of these materials during consecutive soaking and drying in vacuum during the measurement. This effect is of great practical significance as the value of the specific surface influences the electrochemical properties of the conductive polymers [30].

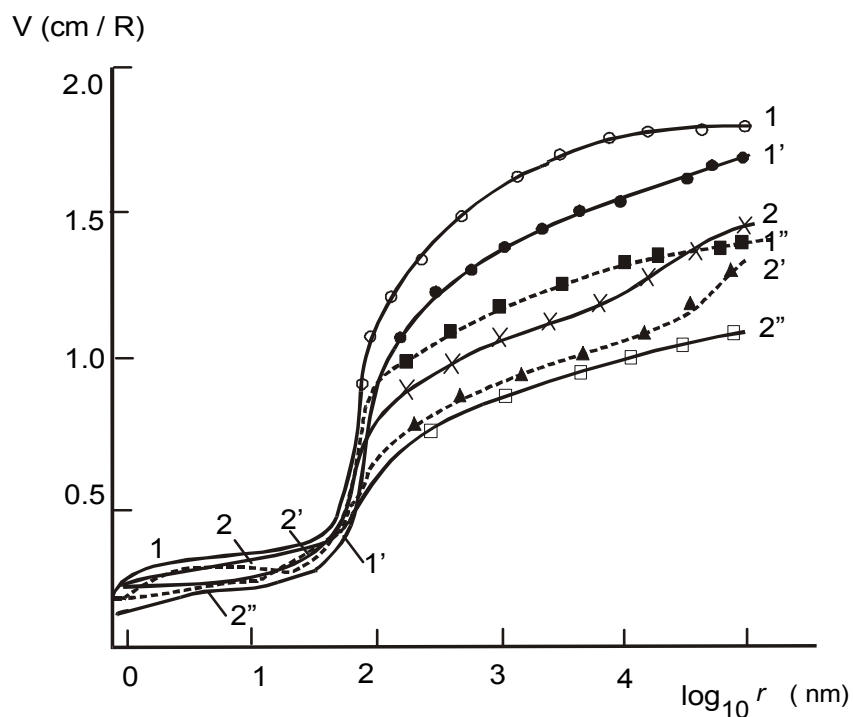


Fig. 17: Integral porograms of (1, 1', 1'') emeraldine chloride and (2, 2', 2'') emeraldine sulfate: (1, 2) first measurement; (1', 2') second measurement; (1'', 2'') third measurement [5].

9.4. Influence of the ion exchange

Fig. 18 shows porograms for an ion-exchange membrane MA-41 in the initial sulfate form (curve 1) and after ion-exchange in dodecyl ether of sulfoacetic acid (curve 2), sodium dodecylsulfate (curve 3), and sodium decylsulfate (curve 4) [31]. One can see that the porous structure depends on the nature of the counter-ion and the pore volume significantly decreases upon transition from inorganic to organic anions.

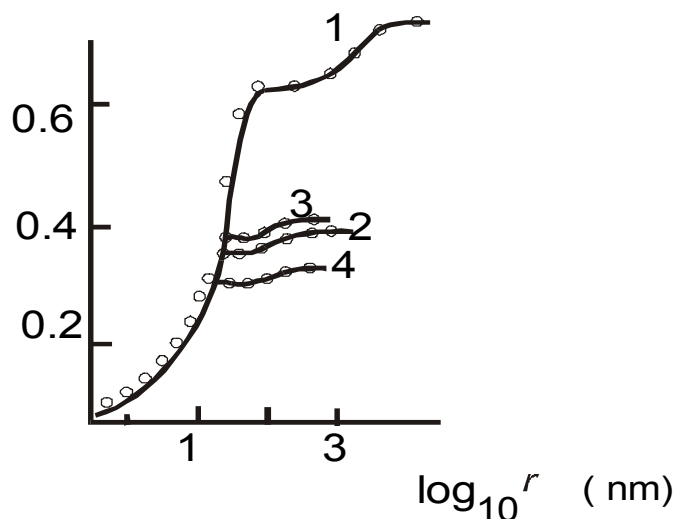


Fig. 18: Integral porograms of the membrane MA-41 stored in different solutions: (1) sodium sulfate; (2) dodecyl ether of sulfoacetic acid; (3) sodium dodecyl sulfate; (4) sodium decyl sulfate [8].

Similar and even more pronounced behavior can be observed with polyaniline in the form of emeraldine salts [32]. In Fig. 19, integral porograms measured with water for chemically synthesized emeraldine chloride (curve 1), and of the same salt after ion exchange in sulfuric and fluoroacetic acid (curves 2 and 3, respectively) are shown. It is evident that the chloride form is substantially more porous than the sulfate form. For the fluoroacetic form in water there is practically no hydrophilic porosity, i.e. this form becomes hydrophobic. The effect of the degree of doping, the nature of counter-ions, and type of the polymerization (chemical or electrochemical) of polyaniline were studied as well [27]. It was shown that all polyaniline forms impregnated with GBL have high porosity of several tenths per cent, high specific surface areas of $80\text{-}400\text{ m}^2/\text{cm}^3$, pore radii of 1-100 nm, and average fibril radii of 2-10 nm.

MSP was applied as well for detailed study of the porous structure and sorption properties of swollen in water Nafion® proton-exchange membranes [33, 34].

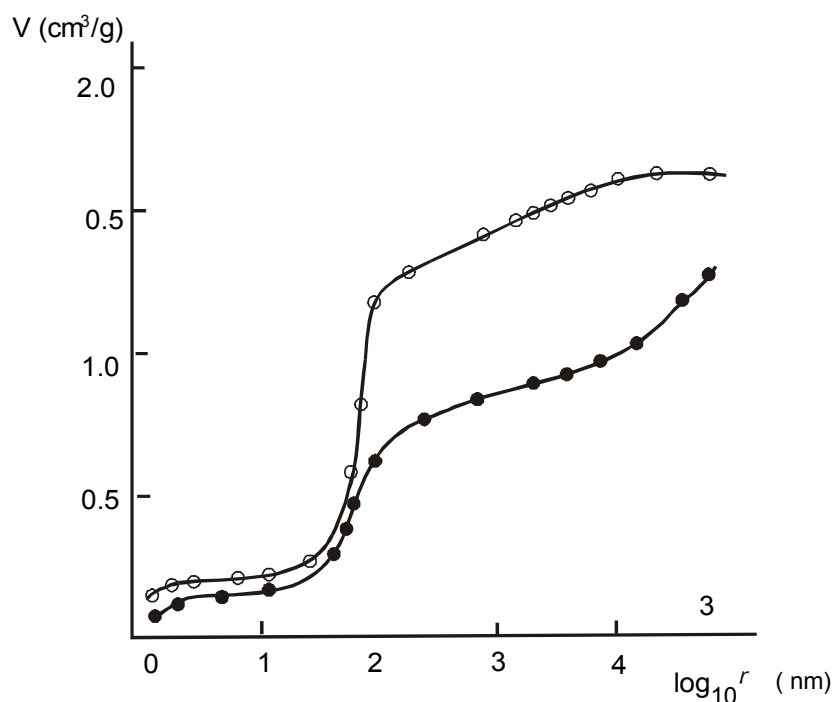


Fig. 19: Integral porograms for salts of emeraldine with the following anions: (1) Cl^- ; (2) HSO_4^- , and (3) CF_3COO^- [9].

9.5. Influence of the pressure on the porous structure

Porous materials are often manufactured by pressing of powders. MSP (unlike MMP) enables studying the structure of porous and dispersed materials at fixed values of pressure. In Fig. 20, porograms of a fixed amount of Raney silver (used as catalyst for oxygen electrodes) at successive increase in pressure are shown. While the pressure rises from 0.05 to 5 Mpa, the volume of the largest pores diminishes, followed by the volume of the smaller pores in the range from $2 \cdot 10^4$ to $3 \cdot 10^2$ nm.

These pores are located between individual particles of the silver catalyst. The structure inside the particles with pores of lower radii (the primary structure) is not altered at these values of pressure. However, when the pressure increases to 10 MPa and higher, a

second stage of compressing is reached corresponding to destruction of the individual particles. In this case the border between the primary and the secondary structures lies at pore radii of about $3 \cdot 10^2$ nm. Thus, MSP gives the possibility to study separately the porous structure of individual primary particles and the secondary structure of particle agglomerates.

Behavior analogous to that in Fig. 20 was observed with other powder samples, e.g., PVC [35].

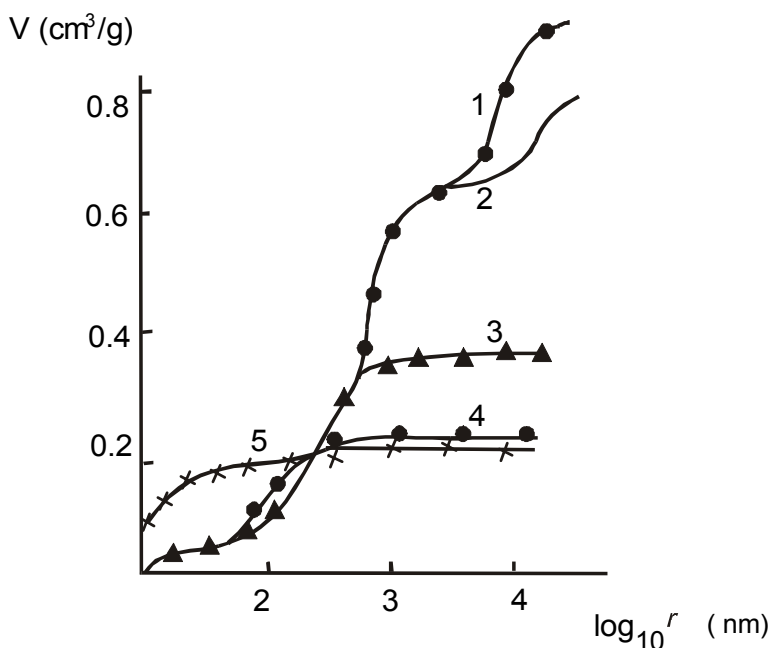


Fig. 20: Integral porograms of pressed Raney silver powder at different pressure (MPa): (1) 0.05; (2) 0.2; (3) 5; (4) 10, and (5) 15.

9.6. Influence of the temperature on the porous structure

In contrast to the method of mercury porosimetry, MSP can be used for studies of the porous structure at different temperatures. For the first time MSP was used for porosimetric measurement of Nafion® proton-exchange membranes swollen in water at elevated temperature (80°C) [33]. A thermostatically controlled cell was used, where high humidity was provided by nitrogen forced through bubbler with water heated to the same temperature in a thermostat. A clamping device (see Fig. 2) was assembled in the cell and used to fix a

specimen with two standards in contact for a time sufficient to achieve capillary and thermal equilibrium.

Fig. 21 gives a comparison of the porous structure of Nafion 117 membrane measured at 20°C (curve 1) and 80°C (curve 2). It can be seen that the heating leads to significant variation of the porous structure, in particular to reduced porosity, only in the region of pores larger than 10 nm [33].

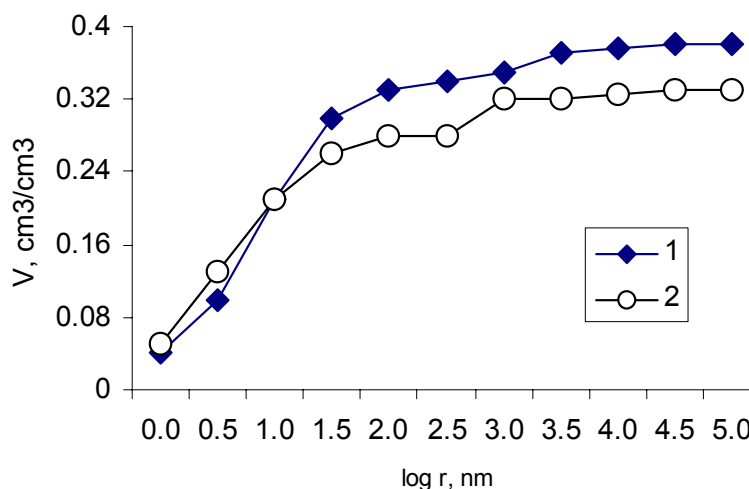


Fig. 21: Integral pore-volume distribution curves vs. radius for Nafion 117 membrane measured at 20°C (1) and 80°C (2) [33].

9.7. Influence of pore-forming agents

When porous products are manufactured by pressing of powders, special additives are often used to increase the amount of large pores or for formation of bi-disperse structures.

The influence of pore-forming agents in titanium electrodes was studied [36]. The electrodes were prepared by pressing powders of titanium and of NH_4HCO_3 (45 μm) at 4.5 MPa and subsequent removal of the pore-forming additive at 100°C. In Fig. 22, porograms measured with decane for different concentrations (weight %, c_p) of the pore-forming agent are shown. It can be seen that the porous structure of the electrode is bi-disperse. Primary structure with pore sizes below 1 μm is formed between the titanium particles and the pore-forming agent forms secondary structure with greater pore sizes. An increase by 1% of the amount of the agent leads to an increase of the pore volume by about 1.1%.

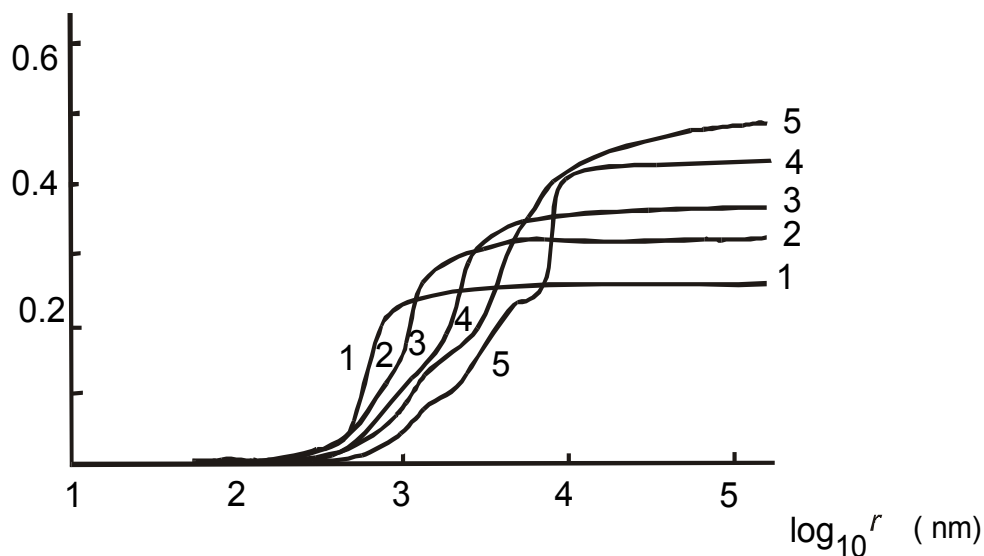


Fig. 22: Integral porograms of titanium electrodes prepared with different concentrations of pore-forming agent: (1) 0 wt. %; (2) 5 wt. %; (3) 10 wt. %; (4) 15 wt. %, and (5) 20 wt. % [11].

These results were obtained by using MSP with evaporation of the working liquid. Therefore they reflect the size of the blocking pores or "necks" r_b between the trapped pores formed by the additive (see section 7). The steep rising sections of the porograms practically correspond to the highest values of r_b . When c_p increases from 5 to 20%, r_b increases from 1.3 to 8 μm though the particle size of the pore-forming agent does not change.

9.8. The structure of dispersed platinum

During measurements of samples of dispersed platinum, e.g. platinized platinum, a large amount of micropores with radii less than 1 nm was found (Fig. 23, curve 1). For platinized platinum these micropores account for more than half of the total pore volume; the radii of most of the remaining pores do not exceed 3 nm. This circumstance is very important since the size of such micropores is comparable with the thickness of the electric double layer, and also with the size of many molecules and ions, especially organic. Both these factors influence adsorption and kinetic properties of the deposits, particularly their intrinsic catalytic activity. Such phenomena were observed in [37-40].

The electrochemical sintering of dispersed platinum polarized at 0.3 V (vs. RHE) in 0.5M H₂SO₄ for several hours was investigated on electrodes prepared by either platinum

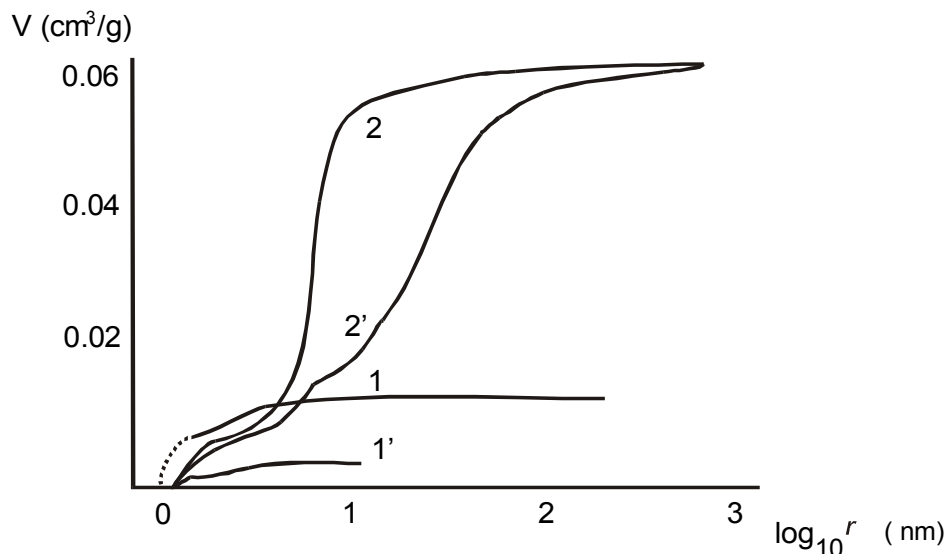


Fig. 23: Integral porograms of (1, 1') platinized platinum and (2, 2') platinum black, (1, 2) before and (1', 2') after electrochemical sintering [16].

deposition on platinum gauze or pressing of platinum black powder at 150 MPa [41]. Fig. 23 shows that for the former sample (curve 1) the average pore size increased from 20 to 40 nm, the specific surface decreased from 28.6 to 17 m²/g and the total porosity decreased more than two-fold. For the latter sample (curve 2) the porosity did not change, the average size of the primary pores increased from 10 to 16 mm and that of the secondary pores - from 20 to 55 mm. The specific surface decreased from 13.8 to 6.5 m²/g. These results show that electrodes prepared from pressed platinum black, unlike electrodes from platinized platinum, have a rigid structure, which prevents shrinkage during polarization.

9.9. Deposition of solids on porous bodies

The structure changes of a carbon-black electrode during thionyl chloride reduction and deposition of LiCl in the pores were investigated [13]. In Fig. 24, porograms obtained at discharge current density 5 mA/cm² down to different values of DOD are shown. It is obvious that the deposition of the reduction products leads to a significant decrease of the larger pores. At the same time a slight increase in the volume of the very small

pores can be observed, which is due to filling of large pores with LiCl crystals. The porosity of the filled pores (which is represented by curve 5 and can be calculated by subtraction of curve 4 from curve 1) is only 3.4%. This dense deposit causes increase in the thickness of the electrode. For electrolytic metal deposition on a porous substrate, different behavior is observed as in this case the deposit is formed not in the bulk of the solution filling the pores but directly at the pore surface. In Fig. 25, porograms of an electrolytically platinized porous titanium electrode are shown [36]. It can be seen that platinizing leads to a shift of the maximum of the distribution curve towards smaller pore sizes and to a gradual lowering of the radii of practically all pores. During platinizing there is a gradual increase of small pores with radii less than 100 nm inside the platinum deposit.

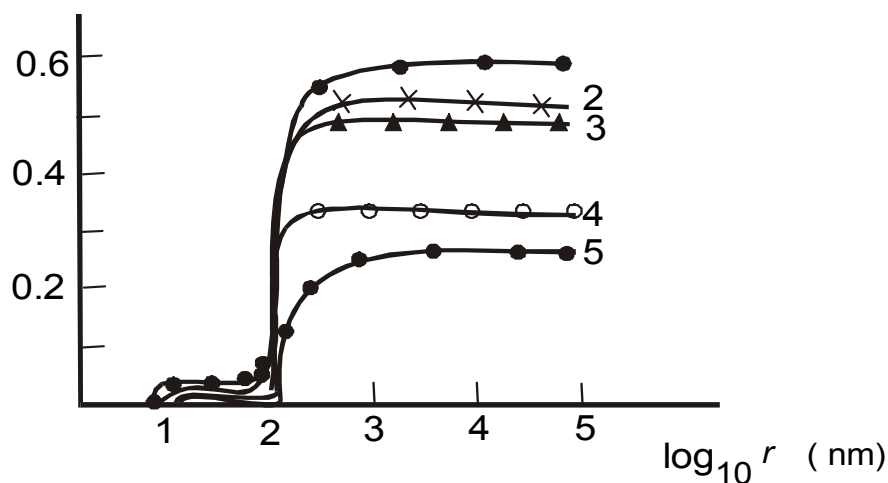


Fig. 24: Integral porograms of a carbon black electrode during thionyl chloride reduction: (1) pristine, (2) at 13% DOD; (3) at 30% DOD; (4) at 100% DOD, and (5) porogram of the deposit [17]. The discharge current density in all cases was 5 mA/cm².

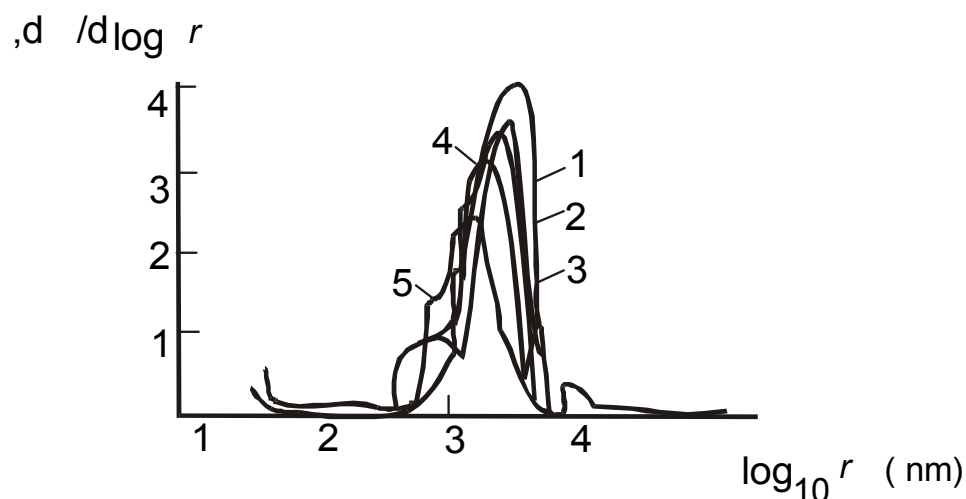


Fig. 25: Differential porograms of a porous titanium electrode (1) before and after platinizing at: (2) 1 min; (3) 3 min; (4) 4 min, and (5) 30 min (11).

9.10. Solid-state reactions in storage cells

Structural changes of the battery electrodes during discharge and cycling is of major importance for better understanding of their properties. As most of the metals employed in such electrodes (lead, cadmium, silver, etc.) are easily amalgamated, MMP is not applicable for this purpose.

From the porogram for the negative electrode of the lead acid cell (Fig. 14) it can be seen that the freshly pasted electrode (curve 1) has a bi-disperse structure with large ratio of pores with radii between 7 and 300 nm and smaller amount of pores between 6 and 10 μm . After formation (curve 2) of the electrode, the main amount of pores corresponds to a narrow range between 800 and 3200 nm while the remainder is spread over the range between 5 and 800 nm. Significant part of the pores in the 800-3200 nm range is kept intact at all states-of-charge of the electrode during cycling. Thus, the main effect of the forming process of lead electrodes is the development of pores in this range. It seems that these pores are important for the transport of HSO_4^- ions, particularly at high current densities. The localization of the structural changes in a narrow range of pore sizes is probably beneficial for the structure reversibility during cycling and thus for enhancing the cycle life of the storage cell. The great

difference of the total porosity in the charged and discharged states is due to the high ratio of the densities of metallic lead and lead sulfate (1.8:1).

For the silver electrode in silver-zinc batteries the main parameter is the efficiency of silver utilization (transformation into AgO) during charging. This efficiency increases with decrease of the charge current density and with increase of the discharge current density. These observations can be compared with structural changes. In Fig. 26, porograms are shown for electrodes manufactured from commonly used silver powder (1, 1') and from fine

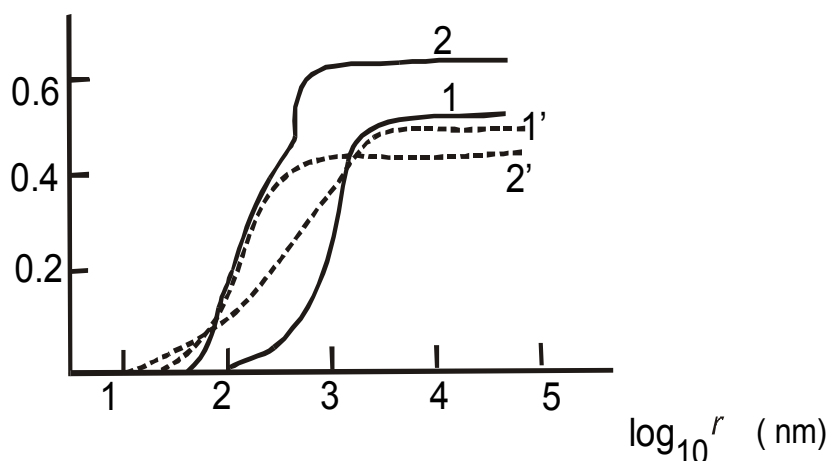


Fig. 26: Integral porograms of silver electrodes prepared from (1, 1') standard silver powder and (2, 2') reduced AgCl, measured (1, 2) before and (2, 2') after formation [42].

grained powder prepared by reduction of AgCl (2, 2'), before formation (1, 2) as well as after formation (1', 2') during two cycles [42]. For the initial electrodes 1 and 2 the values of the specific surface calculated from the porograms were 0.2 and 2.19 m²/g and the efficiencies 47% and 77%, respectively. After formation, the corresponding values were 0.87 and 1.14 m²/g for the specific surface, and 72% and 73% for the efficiency.

Thus, the properties of the electrodes and their structure are leveled after formation. Recrystallization during cycling leads to loss of the "memory" of the initial electrode structure. The increase of efficiency with increasing discharge current density can be attributed to an increase of the specific surface of silver.

MSP was applied to several other materials and processes, namely, polymerization of vinylchloride to polyvinylchloride [35], sintering of porous titanium electrodes [36], storage

of electrodes of the silver-zinc storage cell, preparation of ion-exchange membrane from the corresponding ion-exchange resins [31], etc.

CONCLUSION

A porosimetric method was developed which allows study of all types of porous materials including soft or frail materials and powders. This method is nondestructive and allows repetitive measurements of the same sample. The method can be used for a wide range of pore sizes from 1 to $3 \cdot 10^5$ nm. The use of different working liquids allows evaluation of both wetting angles and water wettability of multi-component porous materials. No complex devices and high pressures are needed for this method. The Method of Standard Porosimetry is now widely used in many scientific and industrial laboratories throughout Russia and other states for investigation of porous materials used in electrochemical devices (electrodes, membranes) as well as of other types of porous materials.

The results obtained by applying the MSP for studies of different processes in batteries, fuel cells and other electrochemical devices are discussed. The following processes were investigated: swelling of ion-exchange polymeric materials (membranes, conducting polymers); pressing of powdered materials (PVC, Raney silver); influence of the temperature on the porous structure; influence of pore-forming agents; chemical and electrochemical sintering of catalysts; deposition of solid products in the pore volume of the cathode during reduction of SOCl_2 in lithium batteries; structural changes during formation and cycling of lead and silver-oxide electrode, etc.

REFERENCES

- [1] I. C. Drake, *Ind. Eng. Chem.*, **41**, 780 (1949).
- [2] M. M. Dubinin, G. M. Plavnik, *Carbon*, **6**, 183 (1968).
- [3] S. Miklos, A. Pohl, *Bergakademie*, **22**, 97 (1970).
- [4] M. Svata, I. Jansta, *Coll. Czech. Chem. Commun.*, **30**, 2455 (1965).
- [5] S. J. Gregg, K. S. W. Sing, "Adsorption, Surface Area and Porosity", Academic Press, New York, 1967.
- [6] G. Rossi, G. Usai, *Quad. Ind. Chim. Ital.*, **6**, 134 (1970).
- [7] A.I. Sarakhov, *Zhurn. Fyz. Khimii*, **37**, 465 (1963).

- [8] M. N. Gavse, "Corrosion and Wettability of Metals by Mercury" [in Russian], Khimiya Publ., Moscow, 1969, 208 pp.
- [9] Yu. M. Volfkovich, E. I. Shkolnikov, V. E. Sosenkin, *Elektrokhimiya*, **14**, 402 (1978);
Yu. M. Volfkovich, V. S. Bagotzky, *J. Power Sources*, **48**, 327 and 339 (1994).
- [10] Yu. M. Volfkovich, V. E. Luzhin, A. N. Vayulin, E. I. Shkolnikov, I. A. Blinov, *Elektrokhimiya*, **20**, 656 (1984).
- [11] Yu. M. Volfkovich, V. E. Sosenkin, *Elektrokhimiya*, **14**, 652 (1978).
- [12] I. A. Blinov, V. E. Sosenkin, Yu. M. Volfkovich, *Elektrokhimiya*, **25**, 395 (1989).
- [13] V. S. Bagotzky, V. E. Kazarinov, Yu. M. Volfkovich, L. S. Kanevsky, L. A. Beketayeva, *J. Power Sources*, **26**, 427 (1989).
- [14] Yu. M. Volfkovich, *Kolloidn. Zhurn.*, **41**, 640 (1979).
- [15] Yu. M. Volfkovich, V. E. Sosenkin, *Dokl. AN SSSR*, **234**, 125 (1977).
- [16] Yu. M. Volfkovich, E. I. Shkolnikov, *Zh. Fyz. Khimii*, **52**, 210 (1978).
- [17] Yu. M. Volfkovich, E. I. Shkolnikov, *Elektrokhimiya*, **15**, 8 (1979).
- [18] Yu. M. Volfkovich, V. S. Bagotzky, V. E. Sosenkin, E. I. Shkolnikov, *Elektrokhimiya*, **16**, 1620 (1980).
- [19] V. M. Matusevich, V. F. Rimskikh, Yu. M. Volfkovich, *Izv. Vyssh. Uchebn. Zavedenii. Neft' i Gaz*, **7**, 5 (1981).
- [20] W. A. Zisman, in: "Contact Angle, Wettability, and Adhesion", *Advances in Chemistry*, Series **43**, Washington D.C., 1964, P.1-56.
- [21] V. L. Sigal, O. A. Mysak, Yu. M. Volfkovich, *Kolloidn. Zh.*, **53**, 1091 (1991).
- [22] Yu. A. Chismadjev, V. S. Markin, M. R. Tarasevich, Yu. G. Chirkov, "Macrokinetics of Processes in Porous Systems" [in Russian], Nauka Publ., Moscow, 1971, 363 pp.
- [23] J. Divisek, Yu. M. Volfkovich, R. Wilkenhoner, Structure of SOFC anode cermets. Part I: Porosity Investigation. *J. Applied Electrochemistry*, **28** (1998) (in press).
- [24] E. S. Livshits, E. G. Yampolskaya, Yu. M. Volfkovich, *Elektrokhimiya*, **19**, 1275 (1983).
- [25] P. M. Dunlap, S. R. Faris, *Nature*, **196**, 1312 (1962).
- [26] Yu. M. Volfkovich, V. S. Bagotzky, T. K. Zolotova, E. Yu. Pisarevskaya, *Electrochimica Acta*, **41**, 1905 (1996).
- [27] Yu. M. Volfkovich, A. G. Sergeev, T. K. Zolotova, S. D. Afanasiev, O. N. Efimov, E. P. Krinichnaya, *Electrochimica Acta*, **44** (1999) 1543.
- [28] Yu. M. Volfkovich, T. K. Zolotova, M. D. Levy, Ya. A. Letuchij, *Adv. Mater.*, **4**, 274 (1993).
- [29] Yu. M. Volfkovich, M. D. Levy, T. K. Zolotova, E. Yu. Pisarevskaya, *Polym. Comm.*, **39**, 2443 (1993).
- [30] Yu. M. Volfkovich, T. K. Zolotova, S. L. Bobe, A. V. Shlepakov, *Elektrokhimiya*, **29**, 897 (1993).
- [31] N. A. Kononenko, N. P. Berezina, Yu. M. Volfkovich, E. I. Shkolnikov, I. A. Blinov, *Zh. Prikl. Khimii*, **58**, 2199 (1985).
- [32] T. K. Zolotova, A. V. Shlepakov, Yu. M. Volfkovich, *Elektrokhimiya*, **29**, 630 (1993).
- [33] J. Divisek, M. Eikerling, V. M. Mazin, H. Schmitz, U. Stimming, Yu. M. Volfkovich, *J. Electrochem. Soc.*, **145** (1998) 2677.
- [34] M. Eikerling, Yu. I. Kharkats, A. A. Kornyshev, Yu. M. Volfkovich, *J. Electrochem. Soc.*, **145**, 2684 (1998).
- [35] V. T. Marinin, D. N. Bort, B. S. Zavyalova, Yu. M. Volfkovich, *Vysokomolekomol. Soyedin., Ser. A*, **22**, 1736 (1980).

- [36] N. V. Kuleshov, Yu. M. Volfkovich, E. L. Fillipov, E. I. Shkolnikov, *Elektrokhimiya*, **14**, 1887 (1978).
- [37] V. F. Stenin, B. I. Podlovchenko, *Vestnik Mosk. Univ., Ser. Khim.*, **4**, 21 (1967).
- [38] O. A. Khasova, Yu. B. Vassilyev, V. S. Bagotzky, *Elektrokhimiya*, **6**, 1367 (1970).
- [39] P. Stonehart, J. Lundquist, *Electrochim. Acta*, **18**, 907 (1973).
- [40] B. I. Podlovchenko, T. D. Gladysheva, O. V. Vyaznikovtseva, Yu. M. Volfkovich, *Elektrokhimiya*, **19**, 424 (1983).
- [41] T. D. Gladysheva, E. I. Shkolnikov, Yu. M. Volfkovich, B. I. Podlovchenko, *Elektrokhimiya*, **18**, 436 (1982).
- [42] V. P. Sirovinskaya, Yu. M. Volfkovich, V. E. Sosenkin, I. E. Yablokova, *Elektrotehnicheskaya Promyshlennost, Ser. Khim. i fis. istochnikov toka*, **6**, 18 (1983).